JJEES

JJEES (2023) 14 (3): 232-240
ISSN 1995-6681

Jordan Journal of Earth and Environmental Sciences

The Use of Remote Sensing and GIS for Mapping Silica Sand Deposits in Jordan

Muheeb Awawdeh, Eman Alkhateeb, Nazem Al-Radaideh*

Dept. of Earth & Environmental Sciences, Yarmouk University-Irbid Jordan

Received 31st May 2022; Accepted 11th May 2023

Abstract

Mining is critical to human development. Today it necessitates cutting-edge spatial technology due to a variety of environmental and social constraints. With free remote sensing data such as Sentinel-2 data from the Copernicus program and EO-1 Hyperion, new study opportunities emerge. The goal of this study was to use remote sensing and GIS techniques to map the silica sand deposits in Jordan. The Energy and Minerals Regularity Commission (EMRC) conducted a field investigation for three sites of silica sand (Ras El-Naqab, Qa' El-Disi, and the Al-Jayoshia).

Samples were collected from the exposed surfaces for laboratory analysis (mineralogy and chemistry). The results confirmed that Si and quartz are the main components of the samples. The spectral signature of silica sand from sampled sites was derived from EO-1 Hyperion and Sentinel-2 images and then compared with the spectral signature from the USGS library.

The spectral signature of the EO-1 Hyperion images was close to the USGS library's spectral signature and then used as training sites for mapping silica sand using the Sentinel-2 images. The end results a map of silica sand in Jordan based on both types of images. The study revealed that southern Jordan is abundant in silica sand more than documented in the literature. The integration of hyperspectral data (EO-1 Hyperion) and multispectral data (Sentinel-2) is an effective approach in mapping Earth minerals meaning that full coverage of the study area with hyperspectral images is not required, eventually, cost savings.

Keywords: *Hyperspectral remote sensing, Silica sand, Sentinel-2, Spectral signature*

1. Introduction

The interpretation and processing of satellite images to extract information and parameters, either qualitatively or statistically, is a cornerstone of remote sensing (Royal Cultural Center, 1995). Multispectral and hyperspectral spectral imaging are two different types of spectral imaging that use comparable technologies. They're different imaging methods in that they each have their own set of applications. Remote sensing for species mapping, mineral exploration, food engineering, agriculture, atmospheric studies, ecology, health care, and agriculture are examples of such application spaces. The acquisition of visible, near-infrared, and short-wave infrared images is part of multispectral remote sensing (USGS, 2021).

A multispectral image gathers image data across the electromagnetic spectrum within a specified wavelength range. At these distinct wavelengths, the various materials collected reflect and absorb differently. It is feasible to distinguish between materials using this imaging technology based on their spectrum reflection fingerprints as seen in these remotely sensed images. Direct identification is impossible as a result. For example, Shamsham and Idries (2022) estimated surface soil particles using remote sensing-based data in Al-Ghab Plain, Syria. Hyperspectral remote sensing, on the other hand, analyzes a broad spectrum of light rather than assigning primary colors to each pixel. Its main purpose is to extract a spectrum from each pixel in a scene image to locate objects, detect processes, and identify materials.

There are numerous benefits to using remote sensing with their various types, including (1) large existing databases such as Landsat, Sentinel-2, and Hyperion, (2) the ability to obtain regional perspectives of large areas, (3) ease of integrating information from multiple sensors, (4) no difficulty or danger in covering remote areas, (5) availability of sophisticated computer analysis software, (6) a wide range of energy ranges (such as infrared, UV, and so on), and (7) It is low-cost and fast. Land use mapping, weather forecasting, environmental and natural hazards investigations, and geological mapping are just a few of the applications that have benefited from remote sensing (Chasmer et al., 2020).

In numerous geological research, such as assessing the damage caused by earthquakes, volcanoes, landslides, floods, and melting in polar regions, remote sensing data is a significant source of information. In mineral exploration research, remote sensing (multispectral and hyperspectral data) has become a significant method for finding and mapping minerals without having to go to the field (Treitz & Rogan, 2004; Ayodele & Ajigo 2020). Jordan is rich in minerals that are well-identified by the Natural Resources Authority (NRA), of Jordan. However, the exact borders of the deposits are not delineated as areas, but as points. Therefore, this study came to use advanced technologies (remote sensing and GIS) to map the areas covered by silica

* Corresponding author e-mail: nazem@yu.edu.jo

sand exactly, which may ease the process of accessibility and investment. Besides, such techniques are rarely used in mineral exploration locally. The study approach is based on utilizing the properties of the electromagnetic spectrum in Sentinel-2 and EO-1 Hyperion imageries.

Silica sand in Jordan is described by its exposure on the surface, effectively mineable by open-pit mining, and low content of impurities and heavy minerals, which means it has a high level of purity that facilitates processing and thus gets high value-added products (Madanat et al., 2014). Silica sand deposits in Jordan, belong to the Disi Sandstone Formation of the lower Ordovician age, and the Kurnub Sandstone Formation of the Lower Cretaceous age which are exposed in the south of Jordan (Figure 1). Some of extremely noteworthy silica sand deposits are known from five sites: Ras El-Naqab, Qa' El-Disi, Wadi Siq, Al Jayoshia area, and Petra. The most important one is Ras El-Naqab (Mohsen, 2016). The layers of silica sand exposed in the areas of Ras El- Naqab and Qa' El-Disi are within the sediments of the Lower Ordovician period while the areas of Al-Jayoshia and wadi Al-Siq are in the rocks of the Lower Cretaceous period. The NRA has estimated the reserves in the Ras El- Naqab area at more than 10 billion metric tons. The local consumption of silica sand is limited to the industries of white cement, ceramics, and plumbing molds (Khoury, 2012).

Madani (2011) mapped the basement rocks and the barite mineralization exposed at the El Hudi area in Egypt using the processed short-wave infrared bands of ASTER. Results showed that garnetiferous muscovite granites have gray image signatures on 5/4 band ratio images whereas pegmatite's and postgranitic dykes have black image signatures. Results at the northern Death Valley site (Kruse, 2013) established that data from the EO-1 Hyperion SWIR spectrometer (2.0 – 2.4 µm) can be used to produce useful mineralogic information. Comparison of EO-1 Hyperion data to airborne hyperspectral data (AVIRIS) shows that EO-1 Hyperion provides the ability to remotely map basic surface mineralogy. Minerals mapped at this site include calcite, dolomite, muscovite, hydrothermal silica, and zeolites. Kryniecka (2015) detected sandbars for a selected section of the Lower Vistula (Wisła) river with the use of Sentinel-2 Level 2A optical images. For multispectral images, water indices were used to separate sandbars from water. The analyses have shown that it is possible to detect sandbars in the river channel based on Sentinel-2 satellite data. Harahsheh (2016) used Landsat-8 to identify and map the lithological units in northern Jordan. She applied different methods including false color analysis and different band ratios to minimize noise fraction, image classification, filtering, and lineament extraction. Ibrahim et al., (2018) utilized samples from drill holes extracted from Tiebaghi, New Caledonia. The chemical composition and the hyperspectral reflectance of each sample were obtained. With the resulting regression models, the mineral chemistry of an outcrop in the vicinity of the drill holes was mapped by a scene of Sentinel-2. The work showed the great potential of free satellite imagery in mapping the chemical characteristics of minerals and rocks. El Atillah et al. (2019) investigated the use of different satellite data, such as Sentinel-2A multispectral imagery, in order to direct the prospection program in an efficient manner, saving both time and cost. The image processing methods of Landsat 7, 8, and the Advanced Spaceborne Thermal Emission and Reflection Radiometer (ASTER) were used to create methods for Sentinel-2A images. The assembly of lithological, structural, and hydrothermal alteration data gave an idea of the mineralogy of the study area. The validity of the results was tested by comparison with the field data and the geological maps of the studied site. Aldiri et al, (2020) provided a comprehensive review of the use of the Landsat-8 and Sentinel-2 multispectral sensors in mineral exploration. Landsat-8 and Sentinel-2 data presented effective and accurate mapping tools for mineral exploration. Both sensors identified iron oxides and Al-OH absorption features, in addition to silicate and carbonate minerals. Alsaleh (2022) assessed the spatial variability of soil properties using hyperspectral remote sensing data, N. Jordan.

2. Methodology

2.1 Samples collection and analysis

Thirty surface samples of silica sand were collected from three sites (Ras El-Naqab, Qa' El-Disi, and Al Jayoshia) defined by the Natural Resources Authority (Figure 1). The samples were randomly selected from each site based on the researcher's field observations taking into consideration surficial features such as color and grain size. The location of samples was recorded by Garmin GPSMAP 60Cx handheld GPS. The samples were undergone wet sieving 100 g of dried sediment was sieved with an aperture of 63 microns to separate mud. The fine fraction (less than 63 m) was then analyzed using an XRD and XRF Analyzer X-ray diffraction and X-ray fluorescence to determine their chemical and mineralogical composition.

2.2 Remote sensing datasets

The current work used the multispectral Sentinel-2A and hyperspectral EO-1 Hyperion remote sensing datasets to map silica sand in Jordan. Eighteen Sentinel-2 images were required to cover the whole country, whereas only 3 Hyperion images were found that partially covered the study area (Figure 2) but were quite enough given the presence of silica sand in the south of Jordan (Table 1).

Table 1. Characteristics of Sentinel-2 and EO-1Hyperion images.

	Sentinel-2	EO-1 Hyperion
Type of sensor	Multispectral	Hyperspectral
Number of bands (range of wavelength)	13 bands (0.4-2.2µm)	242 bands (0.4-2.5 µm)
Number of used scenes	18	3
Spatial resolution	10 - 60 m	30 m
Swath width	290 km	7.7 km

All Sentinel-2 images acquired in August 2020, were downloaded with a radiometric resolution of 16 bits. All bands except band 10 were used for analysis. The sites of sampling areas were used as ground truth points for the classification of the remote sensing data.

2.3 Image pre-processing

Image pre-processing prior to the analysis included geometric correction, radiometric correction, atmospheric correction, mosaicking, and stacking. However, Sentinel-2 images did not need any type of correction. Because of the pseudo projection of EO-1 Hyperion images, the images have been re-projected to UTM Zone 36N. To calibrate and compensate for inaccuracies in the pixel values, the flash tool in ENVI software was used to perform radiometric and atmospheric corrections, because of the improperly calibrated detector on the EO-1 Hyperion push broom scanner (HARRIS, 2021).

Hyperspectral imagers are usually affected by noise during acquisition and transmission (Skauli, 2011; Acito et al. 2011). The imagery, contaminated by noise, may cause failures in information extraction and image interpretation. EO-1 Hyperion has 242 bands. The bands (1-7), (58-76), (225-242) are already set to values of zero (Barry, 2001). Other bands such as (121-126), (167-180), (222-224) have severe noise that corresponds to strong water vapor absorption, so those bands are typically removed from processing (Dat et al, 2003). Minimum noise fraction was used to determine the inherent dimensionality of image data to segregate noise in the data, and to reduce the computational requirements for subsequent processing (Boardman and Kruse, 1994).

Sentinel-2A didn't need radiometric or atmospheric correction because ESA supplies a processor that performs atmospheric correction on Sentinel-2 data with worldwide coverage (Sentinel Hub, 2021). A color composite (stacking) was used to create a single raster from multiple bands of Sentinel-2A and EO-1 Hyperion, then, the mosaic was created using Seamless Mosaic workflow in ENVI software.

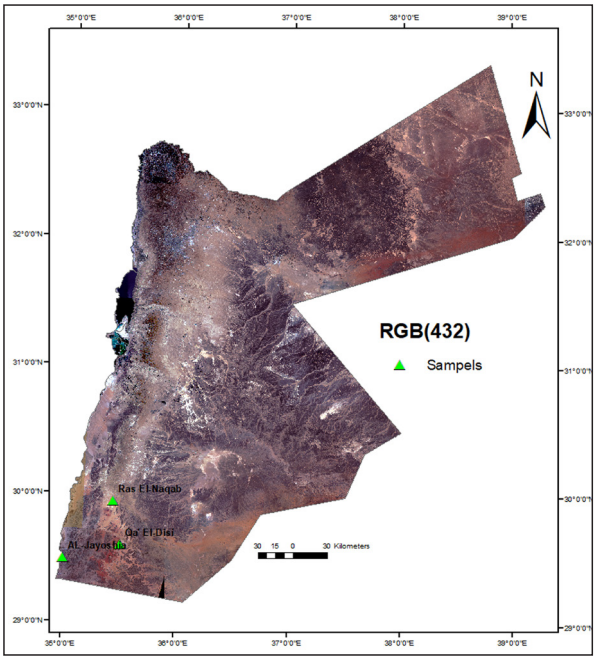

Figure 1. Samples of silica sand superimposed on Sentinel-2 image of Jordan (RGB 432).

2.4 Remote sensing data analysis

Three EO-1 Hyperion images only that were acquired during the period 2002-2005 were available for free from the USGS (2021) (Table 2 and Figure 2).

Table 2. EO-1 Hyperion scenes used to read the electromagnetic signatures.

Scene number	Id	Acquisition Date
Scene1	EO1H1740382003253110KZ	10 September 2003
Scene2	EO1H1740392002275110PY	2 October 2002
Scene3	EO1H1740392005258110KK	15 September 2005

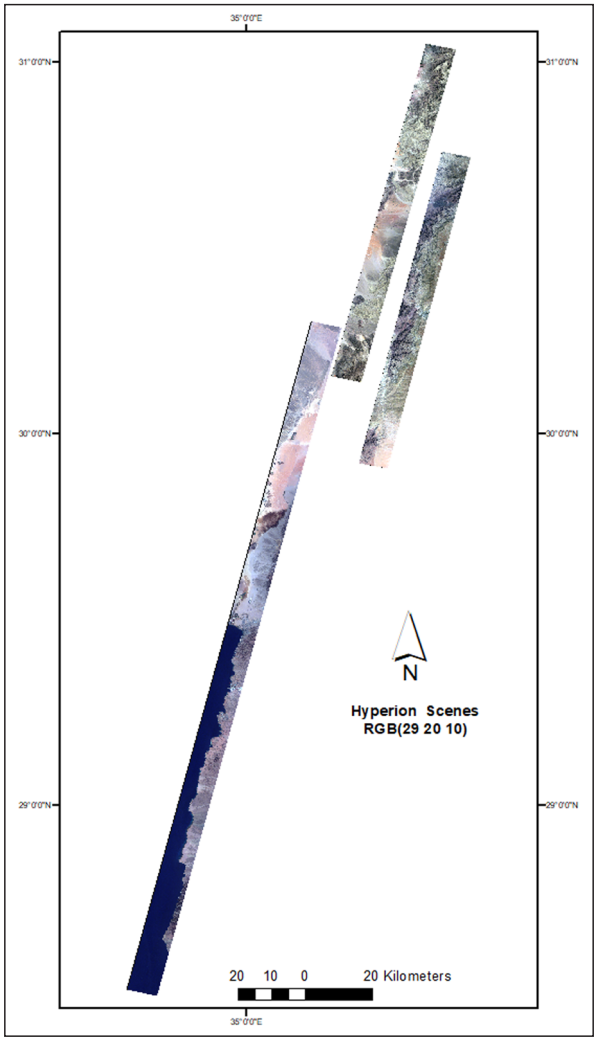

Figure 2. The EO-1 Hyperion images used in this study with true colors RGB (29 20 10).

Kuching (2007) found that the most accurate method of classification of hyperspectral images was maximum likelihood classification. Therefore, the Hyperion images were classified using this method. But, before classification, matched filtering (MF) was adopted to find the abundances of endmembers such as silica sand using partial unmixing.

This method of supervised categorization necessitates the selection of a target region (ROI). The sampled sites were in the province of Scene 1 (Table 2) of the EO-1 Hyperion images from which the electromagnetic spectrums were captured and used as training sites for the mapping silica sand zones in all scenes of the Hyperion images. The color composite RGB (29 20 10) was chosen to read the electromagnetic signature. The large number of bands in the EO-1 Hyperion images increases the ability to distinguish the desired minerals. The more bands, the more pronounced the curve (the signature).

On the other hand, it was not possible to identify the characteristic features clearly by using Sentinel-2. This is due to the very limited number of bands and the adsorption/ reflectance features were concentrated at 0.9 micrometers and less (ESA, 2021). To distinguish silica sand, absorption will appear around wavelengths of 1.4 micrometers and 1.9 micrometers due to its hydroxide content (Viallefont-Robinet, 2019).

A supervised classification has been used. Scene 1 of the EO-1 Hyperion satellite was classified based on its mineral content according to Alnawafleh et al. (2013) mineral map (Figure 3). The second step was to utilize the zones of silica sand identified from the Hyperion images as training sites for Sentinel-2 images, bearing in mind that Sentinel-2 images cover the whole country. The ROI (region of interest) was taken in Sentinel-2 Jordan images based on the silica sand zones that were obtained from the classification of the Al-Jayoshia image of the EO-1 Hyperion satellite, in addition to the locations of samples of clay minerals that were taken and analyzed during the field study and based on the mineral map of Jordan from Alnawafleh et al. (2013).

To affirm the results of the mapping, validation was carried out using two methods:(1) Validation using electromagnetic spectrum: The spectral signature from mapped zones of silica sand based on either image (Sentinel-2 or Hyperion) could be compared with the signature of the silica from the USGS library, and (2) Validation using Google Earth: Google Earth was used to ascertain the nature of the areas where silica sand was mapped by visual interpretation and feasible areas for mining. A further step was carried out for comparison purposes. The mapped zones of silica sand from both sensors were intersected to find out the extent of overlap areas

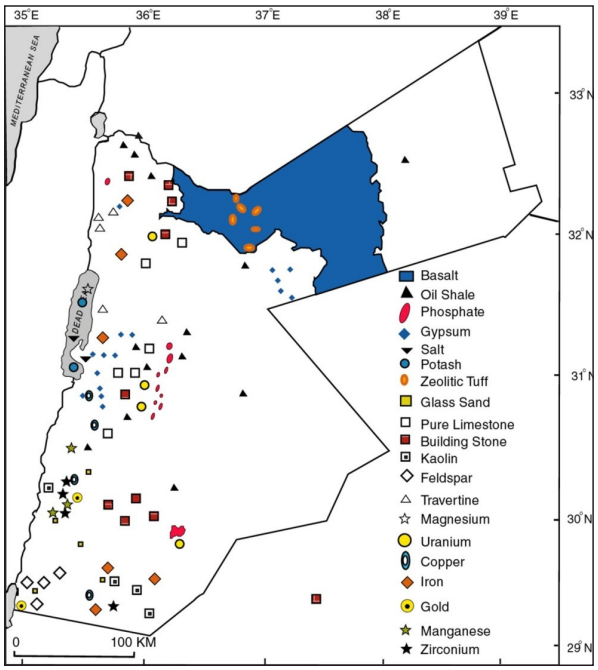

Figure 3. Jordan mineral map (Alnawafleh et al. 2013).

3. Discussion and Results.

3.1 XRF and XRD analysis

The fine fraction of silica sand from Ras El-Naqab region, Qa' El-Disi, and AL-Jayoshia (Figure 4) contain quartz as the major mineral and very minor amounts of calcite, berlinite, despujolsite, and algodonite, (Table 3 and Figure 4). These minerals have been previously linked to quartz.

Table 3. XRF analysis for Ras El-Naqab, Al Jayoshia, and Qa' El-Disi sediments.

Sample site	SiO_2%	Cl %	CaO%	TiO2%	K_2O%	Fe_2O_3%	Total%
Ras El-Naqab	97.8	0.85	0.37	0.39	-----	0.15	≈100%
Qa' El-Disi	83.45	-------	4.23	1.69	4.96	5.54	≈100%
Al Jayoshia	86.97	6.87	4.32	0.60	-----	1.16	≈100%

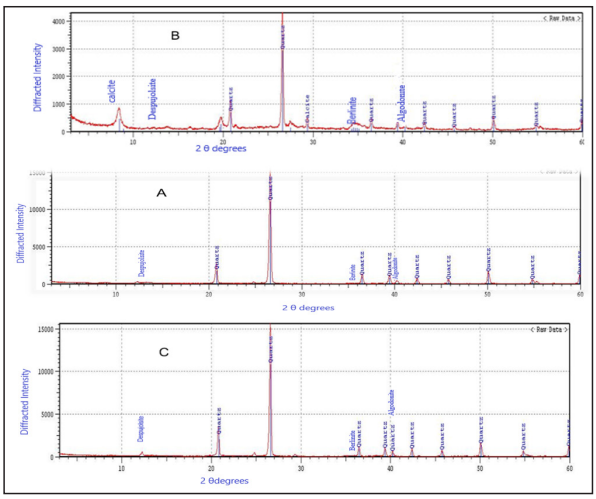

Figure 4. XRD diagram analysis of <63 micron for (A) Ras El-Naqab, (B) Qa' El-Disi and (C) Al-Jayoshia sediments.

The highest proportion of SiO2 was found in Ras El-Naqab (97.80%), followed by the AL-Jayoshia area (86.90%) and Qa' El-Disi (83.45%). The existence of impurities, notably in the form of iron, titanium, and calcium oxides, accounts for the varying percentages. The most important impurity is iron oxide. These contaminants present significant challenges in a variety of applications, including the manufacture of colorless or optical glass, optical fibers, and high-purity ceramics (Chammas, 2001).

Iron (III) oxide percentages were 0.15 % in Ras El-Naqab, 1.16 % in Al-Jayoshia, and 5.54 % in Qa' El-Disi. These results are good, according to EMRC (2014), when considering that the samples were obtained from the surface and evaluated in their natural state, which usually yields a larger percentage of contaminants. Chemical weathering rises as a result of this exposure, resulting in a high percentage of impurities such as iron (III) oxide.

When comparing our XRF findings to those of the EMRC study (2019), it is found that SiO2 and Fe2O3 concentrations are98.72 % and 0.04 %in Ras El- Naqab, and 96.5 % and 0.025 %, in Qa' El-Disi, respectively. The higher quality of silica sand obtained by the Energy and Minerals Regularity Commission (EMRC) is attributed to the subsurface samples and samples washing by wet sieving.

3.2 Spectral signature analyses of silica sand

The signatures of three silica sand samples from Ras El-Naqab, Al-Jayoshia, and Qa' El-Disi are represented by Sentinel-2 spectrum signatures (Figure 5). The signature from these samples was insufficient to determine the mineral composition because it only reveals the spectrum absorption of the iron (III) oxide.

Therefore, high spectral resolution data is essential for this purpose, and hyperspectral technologies play a vital role in this regard. One sample only (Al-Jayoshia) was found within the spatial extent of EO-1Hyperion images (scene 1), just (Figure 1). Its spectral signature was extracted and compared to that of silica sand from the USGS library (Figure 6).

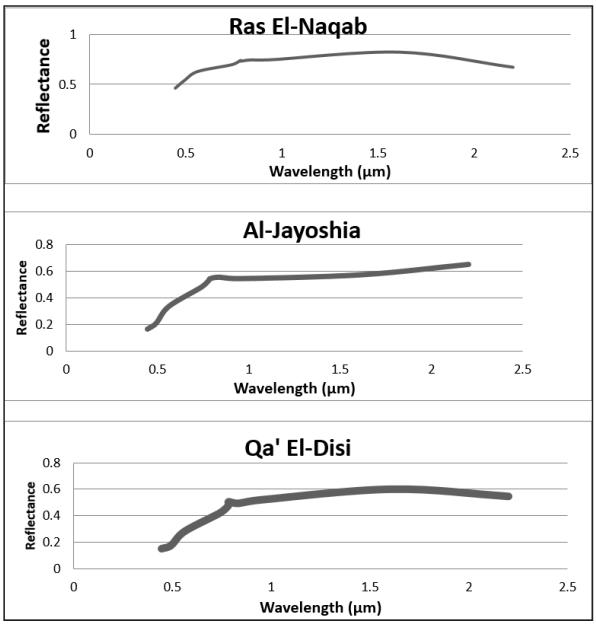

Figure 5. Sentinel-2 spectral signature for Ras El-Naqab (a), Al-Jayoshia (b), and Qa' El-Disi (3). The absorption around 0.9 µm is for iron oxide.

The signature in EO-1 Hyperion images had spectral signature behavior similar to that of a silica sand signature from the USGS library, taking into account the number of bands, where the library spectrum has 3375 bands, whereas the number of Hyperion bands used is only 175 due to the removal of some bands with zero values. The USGS library's silica sand spectral profile (Figure 6) revealed absorptions at 0.9, 1.4, and 1.9 µm. The quantity of the element or compound that triggered the absorption is proportional to the depth of absorption. The absorption patterns around 0.9 to 1.2 µm were caused by iron oxide concentration, whereas the absorption features around 1.4 to 1.9 µm were caused by the hydroxide ion trapped in the silicates, which form a characteristic silica sand impression. Clay minerals and carbonate content are responsible for the absorption properties between 2 and 2.5 µm. The EO-1 Hyperion image (scene 1) was categorized using the extracted spectral signature based on the maximum likelihood method (Figure 7). The identified zones of silica sand from this process were used as training sites for Sentinel-2 classification (Figure 8). The last step was using the mapped zones of silica sand from the Sentinel-2 images as training sites for the classification of the other two EO-1Hyperion images (Scene2) and (Scene3) (Figure 9). The spectral signatures of the mapped zones of silica sand from these images were investigated against signatures of silica sand from the USGS library.

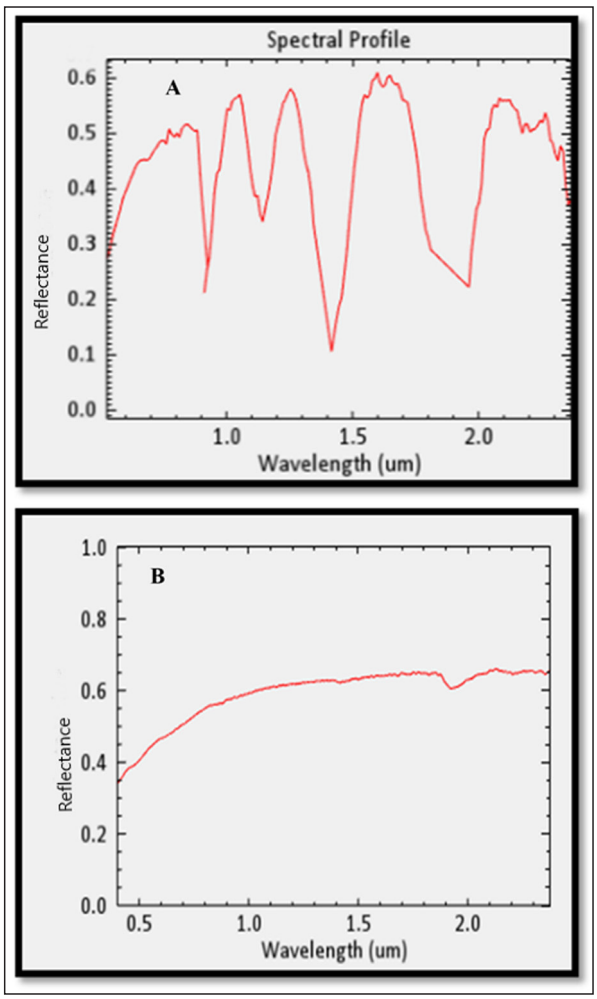

Figure 6. Spectral signature from (Scene1) EO-1Hyperion image (A) with spectral signature for silica sand from the USGS library (B).

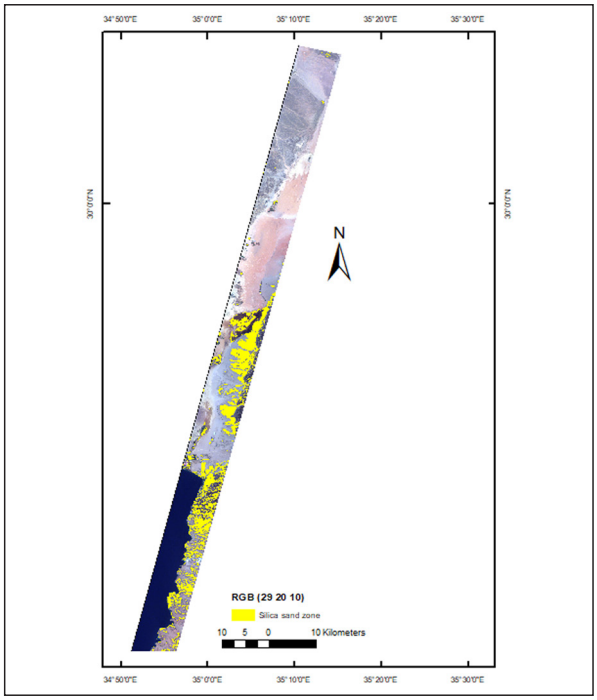

Figure 7. Silica sand zones (yellow color) extracted from EO-1 Hyperion image (scene 1).

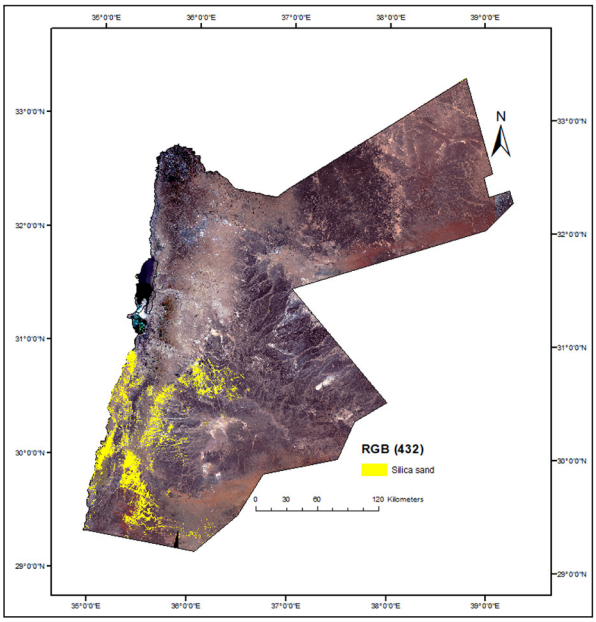

Figure 8. Silica sand zones (yellow color) extracted from Sentinel-2.

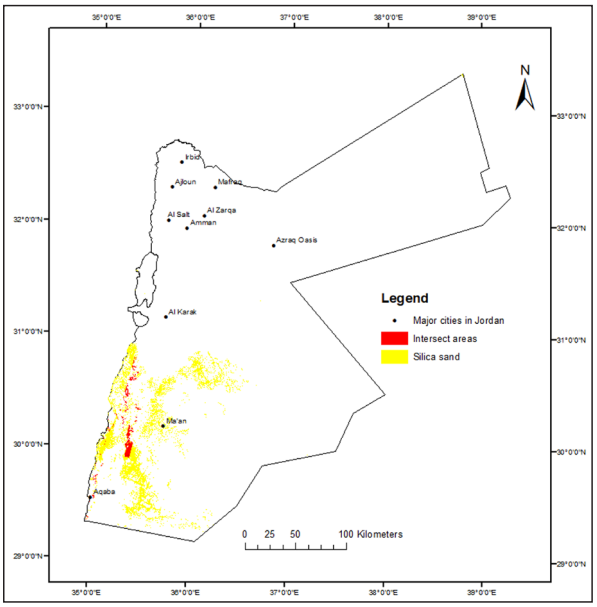

Figure 10. Intersect results of overlaying Sentinel-2 and EO-1 Hyperion silica sand zones.

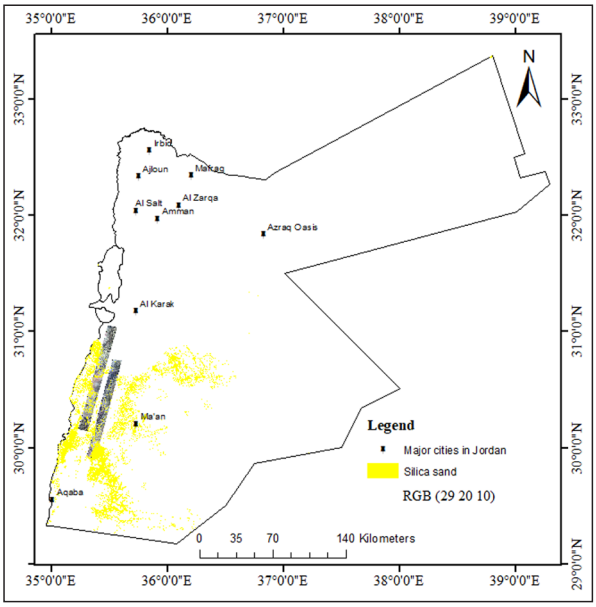

Figure 9. Silica sand zones extracted from Sentinel-2 image overlay EO-1Hyperion images (scenes 2 and 3).

Figure 11. Prospected silica sand in Qa' El-Disi (a), Ras El-Naqab (b) as seen on Google Earth.

3.3 Validations of results

The existence of silica sand was established by comparing the electromagnetic spectrum from the mapped areas, which was very close to the silica sand spectrum from the USGS library (Figure 6). An overlay GIS operation was carried out to calculate the degree of intersection (overlap) between zones of silica sand from both images (Hyperion and Sentinel) (Figure 10) and found to be 57 %, meaning that these zones were identified using both images. Considering the disparities in image characteristics (spectral and spatial resolution), the outcome is considered acceptable. Moreover, the visual interpretation of Google Earth images (Figure 11) indicated the presence of silica sand in terms of texture, brightness, topography, and land cover. Size from 50.2 km^2 in Qa' El-Disi to 72.7 km^2 in Ras El-Naqab.

Matched Filtering (MF) is also used to validate work by finding the abundance of user-defined endmembers using a partial unmixing. This technique maximizes the response of the known endmember and suppresses the response of the composite unknown background, thus matching the known signature. It provides a rapid means of detecting specific materials based on matches to library or image endmember spectra and does not require knowledge of all the endmembers within an image scene. The Matched Filter (MF) produced a succession of grayscale images, one for each endmember specified (silica sand). In the Hyperion photos, silica sand appeared as bright zones in the higher tail of the histogram (Figure 12).

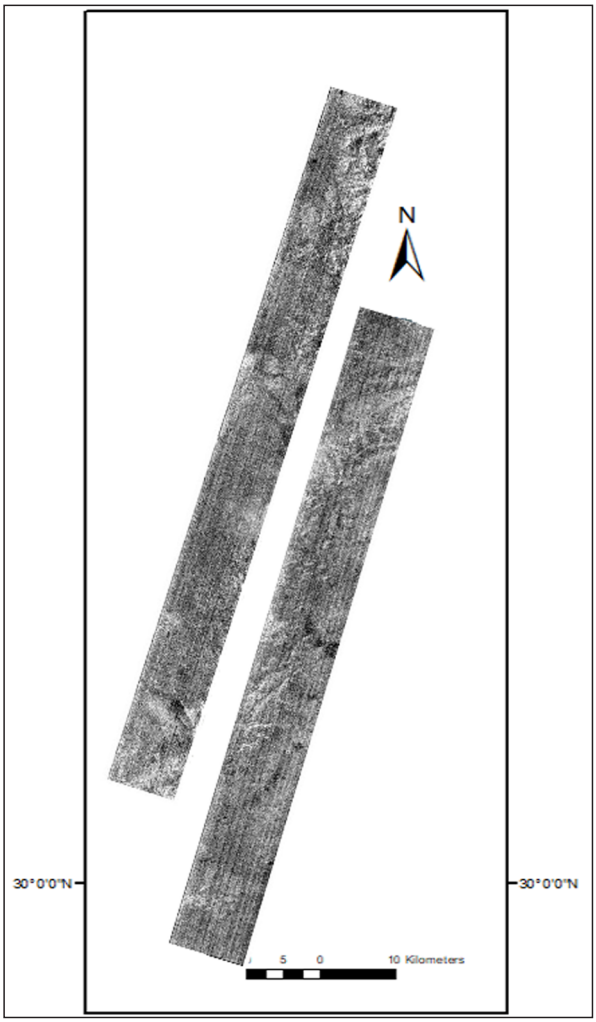

Figure 12. Matched filter for hyperspectral images from EO-1 Hyperion (scene 2, scene 3). Silica sand determine as endmember. Silica sand appears as bright areas.

3.6 The spectral signature and mineral content

The absorptions areas at 0.9 µm and 1.2 µm refer to the iron oxide, 1.4 µm and 1.9 µm absorption are due to OH or H2O, whereas absorptions at 2.0 µm to 2.5 µm at Qa' El-Disi, Al-Jayoshia, and Ras El-Naqab are indicators of clay minerals and carbonates. These absorptions in Qa' El-Disi, Al-Jayoshia, and Ras El-Naqab were different in the electromagnetic spectrum (Figure 13). The greatest iron oxide ratio was 5.45% in Qa' El-Disi, followed by 1.16% in Al-Jayoshia, and 0.15 % in Ras El-Naqab. These iron oxide ratios are related to color changes in samples that can be seen visually. The higher the iron oxide level, the darker the red hue. The shape of the signature is affected by the quantity of iron oxides; the higher the concentration of iron oxides, the higher the absorption rate at 0.9 µm to 1.2 µm in the spectral profile. The absorption of iron oxides in the Al-Jayoshia area appears to be stronger than in the Ras El-Naqab area. The quantity of clay minerals and carbonate also impacts the shape of the spectral signature; the more clay minerals and carbonate in the spectral profile, the higher the absorption rate at 2.0 µm to 2.5 µm. The percentage of carbonate in Ras El-Naqab was 0.37 %, while it was 4.32 %in Al-Jayoshia.

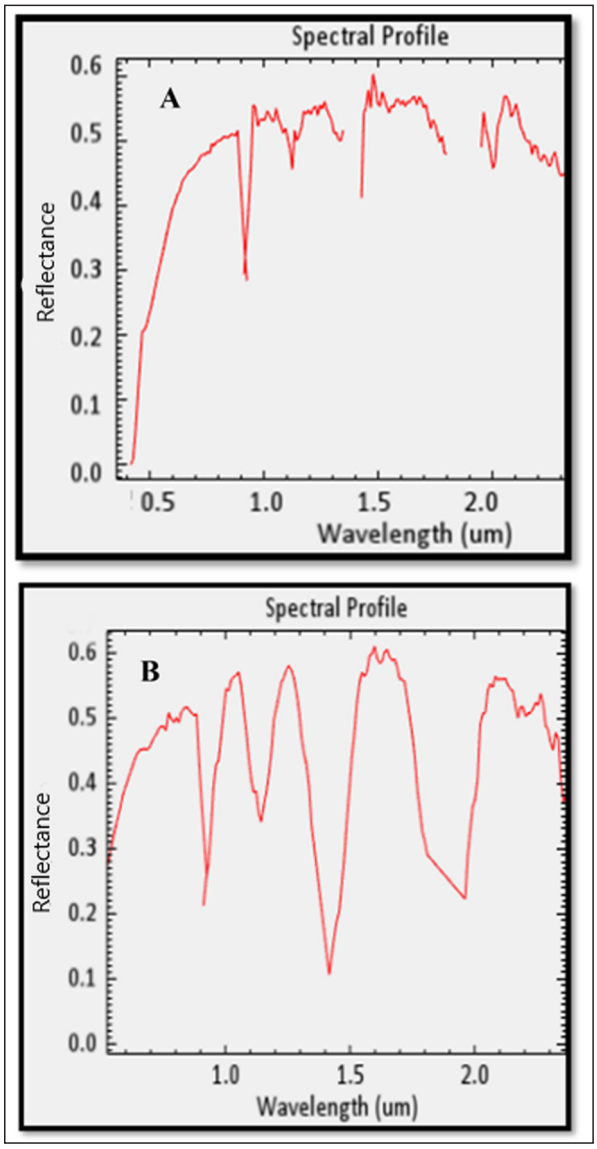

Figure 13. (A) Spectral profile for Ras El-Naqab. The absorption rate was down to (2.9) at0.9µm and to (4.4) at 2.3µm, (B) Spectral profile for the Al-Jayoshia region, with absorption down to (2.1) at 0.9µm and to (3.4) at 2.3µm.

4. Conclusion

This study employed hyperspectral EO-1 Hyperion and multispectral Sentinel-2 data to map silica sand in Jordan. Field investigation of known verified locations was used as reference points (Ras El-Naqab, Qa' El-Disi, and the Al-Jayoshia) in this study. Samples were obtained from the exposed surfaces and analyzed in the lab for the mineral content and chemical composition. The results showed that quartz and silica are the predominant materials in all sites. The presence of impurities such as iron oxides accounts for the varied percentages, which are 0.15 % in Ras El-Naqab, 1.16 % in Al-Jayoshia, and 5.54 % in Qa' El-Disi. These results are good indicators that Ras El- Naqab is promising for silica sand mining.

This study proved the potential integration of hyperspectral data and multispectral remote sensing data for mineral mapping. The large coverage by Sentinel 2 benefited from the high-resolution data from Hyperion for mapping the silica sand in Jordan. Despite the noise in the EO-1 Hyperion data, we were able to map silica sand after image

processing. This approach saves the cost of acquiring costly hyperspectral data. However, map validation samples must be collected and analyzed. Remote sensing data is useful for mapping minerals because it eliminates field labor and the need for large numbers of samples to be analyzed. The study confirmed the presence of silica sand in south Jordan, but with larger areas, at least 89 km2. This may shed light on the potential mining of silica sand which can be used in a variety of industries due to its surface exposure and ease of access, as well as its high purity in the natural environment. Other tools and techniques can be applied in this area of research such as the use of thermal bands field spectroradiometer.

Acknowledgments

This research has been supported by the Deanship of Scientific Research and Graduate Studies, Yarmouk University (Grant No. 52/2020).

References

Ababsa, M. ed., 2013. Atlas of Jordan: history, territories and society (Vol. 32).

Abdelhamid, G., 1990. The Geology of Jabal Umm Ishrin Area (Wadi Rum), Map Sheet No. 3049II. Bulletin 14, Natural Resources Authority, Geological Directorate. Map Division, Amman.

Abu Halima, K., 1993. Mineralogy, chemistry and industrial studies of Al-Yamaniyya clay deposits in Aqaba area. Unpublished M.Sc. Thesis, The University of Jordan, Amman.

Adiri, Z., Lhissou, R., El Harti, A., Jellouli, A. and Chakouri, M., 2020. Recent advances in the use of public domain satellite imagery for mineral exploration: A review of Landsat-8 and Sentinel-2 applications. Ore Geology Reviews, 117, p.103332.

Acito, N., Diani, M. and Corsini, G., 2011. Signal-dependent noise modeling and model parameter estimation in hyperspectral images," IEEE Transactions on Geoscience Remote Sensing, vol. 49, no. 8, pp. 2957–2971, Aug. 2011.

Al Kuisi, M., Abed, A.M., Mashal, K., Saffarini, G. and Saqhour, F., 2015. Hydrogeochemistry of groundwater from karstic limestone aquifer highlighting arsenic contamination: case study from Jordan. Arabian Journal of Geosciences, 8(11), pp.9699-9720.

Aladaileh, H., Al Qinna, M., Karoly, B., Al-Karablieh, E. and Rakonczai, J., 2019. An investigation into the spatial and temporal variability of the meteorological drought in Jordan. Climate, 7(6), p.82.

Al-Ansari, N., Ibrahim, N., Alsaman, M. and Knutsson, S., 2014. Water demand management in Jordan. Engineering, 6(1), pp.19-26.

Al-Homoud, A.S. and Tat, A.B., 1997. Engineering geology of the Aqaba-Ras El Naqab highway re-alignment, Jordan. Engineering geology, 47(1-2), pp.107-148.

Anthony, J.W., 1990. Handbook of mineralogy: Arsenates, phosphates, vanadates. Arsenates, phosphates, vanadates, 4. Mineral Data Pub.

Alsaleh, A. 2022. Assessing the Spatial Variability of Soil Properties Using Hyperspectral Remote Sensing Data, N. Jordan. M.Sc. Thesis. Department of Department of Earth and Environmental Sciences, Yarmouk University, Jordan.

Ayodele, O. and Ajigo, I. (2020). Geological Mapping and Gemstones prospecting in Deformed Precambrian Rocks, East of Okemesi Fold Belt, Southwestern Nigeria. Jordan Journal of Earth and Environmental Sciences, 11(4) 290-301.

Baker, M.B., 2017. The Application of Marble and Granite as Building Materials in Jordan. Jordan Journal of Civil Engineering, 11(2), pp.234-238.

Bannari, A., El-Battay, A., Bannari, R. and Rhinane, H., 2018. Sentinel-MSI VNIR and SWIR bands sensitivity analysis for soil salinity discrimination in an arid landscape. Remote Sensing, 10(6), p.855.

Barkley, M.C., Yang, H., Evans, S.H., Downs, R.T. and Origlieri, M.J., 2011. Redetermination of despujolsite, Ca3Mn4+ (SO4) 2 (OH) 6· 3H2O. Acta Crystallographic a Section E: Structure Reports Online, 67(9), pp.i47-i48.

Barry, P., 2001. EO-1/Hyperion science data user's guide, Level 1_B. TRW Space, Defense & Information Systems, Redondo Beach, CA, Rep. HYP. TO, 1.

Barry, R., Sawada, Y. and Kabeto, K., 1998. Crushing performance and contamination tdals of a tungsten carbide ring mill compared to agate grinding. Geoscience ReptShimane Univ (17), pp.1-9.

Bayook, A., 1992. Batn El Ghoul Deposits as a Potential Source for Aluminum (Doctoral dissertation, M. Sc. Thesis, University of Jordan).

Bender, F., 1974. Geology of Jordan. Berlin: Gebrüder Borntraeger.

BMS factories., 2019. [https://www.bm.com.sa/ar], [Date of visit12/13/2021].

Brimhall, G.H., Dilles, J.H. and Proffett, J.M., 2006. The role of geologic mapping in mineral exploration: Society of Economic Geologist Special Publication 12.

Boardman, J. W., and Kruse, F. A., 1994. Automated spectral analysis: A geological example using AVIRIS data, northern Grapevine Mountains, Nevada. Proceedings of the Tenth Thematic Conference on Geologic Remote Sensing, San Antonio, TX,9–12 May1994, (Ann Arbor, MI : ERIM), pp. 1 – 407 – 1 – 418 .

Castaldi, F., Palombo, A., Santini, F., Pascucci, S., Pignatti, S. and Casa, R., 2016. Evaluation of the potential of the current and forthcoming multispectral and hyperspectral imagers to estimate soil texture and organic carbon. Remote Sensing of Environment, 179, pp.54-65.

Chammas, E., Panias, D., Taxiarchou, M., Anastassakis, G.N. and Paspaliaris, I., 2001. Removal of iron and other major impurities from silica sand for the production of high added value materials. In Proceedings of the 9th Balkan Mineral Processing Congress, İstanbul.

Chasmer, L., Cobbaert, D., Mahoney, C., Millard, K., Peters, D., Devito, K., Brisco, B., Hopkinson, C., Merchant, M., Montgomery, J. and Nelson, K., 2020. Remote sensing of boreal wetlands 1: data use for policy and management. Remote Sensing, 12(8), p.1320.

Datt, B., McVicar, T.R., Van Niel, T.G., Jupp, D.L. and Pearlman, J.S., 2003. Preprocessing EO-1 Hyperion hyperspectral data to support the application of agricultural indexes. IEEE Transactions on Geoscience and Remote Sensing, 41(6), pp.1246-1259.

El Atillah, A., El Morjani, Z.E.A. and Souhassou, M., 2019. Use of the Sentinel-2A Multispectral Image for Litho-Structural and Alteration Mapping in Al Glo'a Map Sheet (1/50,000) (Bou Azzer–El Graara Inlier, Central Anti-Atlas, Morocco). Artificial Satellites, 54(3), pp.73-96.

ESA. 2021. [https://sentinel.esa.int/web/sentinel/missions/sentinel-2], [date of visit 20/10/2020].FIS.2020.

[https://www.fis.uni-bonn.de/en/recherchetools/Infobox/professionals/resolution/radiometric-resolution], [date of visit 10/2/2021].

Fomin, D.S., Valdes-Korovkin, I.A., Holub, A.P. and Yudina, A.V., 2019. Dry sieving analysis of soil by vibratory sieve shaker: modification and optimization. Bulletin of VV Dokuchaev Soil Science Institute, 96, pp.149-177.

FPDF. 2008. [www.fpdf.org], [date of visit12/6/2021].

Galvão, L.S., Formaggio, A.R., Couto, E.G. and Roberts, D.A., 2008. Relationships between the mineralogical and chemical composition of tropical soils and topography from hyperspectral remote sensing data. ISPRS Journal of Photogrammetry and Remote Sensing, 63(2), pp.259-271.

Haddadin, M., 1974. Possibilities of bentonite in Jordan. In Natural Resources Authority (NRA) Internal Report, p. 24.

Harahsheh, R., 2016. Geological mapping using remote sensing and GIS technique case study in Umm-Qais–Northern Jordan. MSc thesis. The Hashemite University, Zarqa, Jordan, p.65.

HARRIS.2021. [https://www. l3harrisgeospatial.com /docs/ Hyperionvegetationanalysistutorial.html], [date of visit 8/2/2021].

Harsanyi, J.C. and Chang, C.I., 1994. Hyperspectral image classification and dimensionality reduction: An orthogonal subspace projection approach. IEEE Transactions on geoscience and remote sensing, 32(4), pp.779-785.

Humboldt State University. 2019. [gsp.humboldt.edu], [date of visit 6/1/2020].

Ibrahim, K.M., Moh'd, B.K., Masri, A.I., Al-Taj, M.M., Musleh, S.M. and Alzughoul, K.A., 2014. Volcanotectonic evolution of central Jordan: Evidence from the Shihan Volcano. Journal of African Earth Sciences, 100, pp.541-553.

Khallouf A., Shamsham, S., and Idries Y. (2022). Estimation of Surface Soil Particles Using Remote Sensing-based Data in Al-Ghab Plain, Syria. Jordan Journal of Earth and Environmental Sciences, 13 (1): 26-36.

Khoury, H. N., 2019. Industrial rocks and minerals of Jordan: a review. Arabian Journal of Geosciences, 12(20), p.619.

Khoury, H. N., 2019. Review of clays and clay minerals in Jordan. Arabian Journal of Geosciences, 12(23), p.706.

Khoury, H., 2006. Industrial rocks and minerals in Jordan. Publications of the Deanship of Academic Research. The University of Jordan, Amman.

Khoury, H., 2012. Glass sand in Jordan. Publications of the Deanship of Academic Research. The University of Jordan, Amman.

Kruse, F.A (2004) Mineral Mapping with AVIRIS and EO-1 Hyperion. Proceedings of the 12th JPL Airborne Earth Science Workshop, Pasadena, CA, 2004.

Kryniecka, K. and Magnuszewski, A., 2020. USE OF SENTINEL-2 IMAGES FOR THE DETECTION OF SANDBARS ALONG THE LOWER VISTULA. Acta Scientiarum Polonorum. Formation Circumiectus, 19(2), pp.23-33.

Kurnia, G., Yulianto, B., Jamari, J., Bayuseno, A.P. and Tauviqirrahman, M., 2020, September. Contact mechanism between shaft, key, and crank in the sand sieving machine. In AIP Conference Proceedings 2262(1), p.030015. AIP Publishing LLC.

Machado, G.S., Groszewicz, P.B., de Freitas Castro, K.A.D., Wypych, F. and Nakagaki, S., 2012. Catalysts for heterogeneous oxidation reaction based on metalloporphyrins immobilized on Kaolinite modified with triethanolamine. Journal of colloid and interface science, 374(1), pp.278-286.

Madanat, G.M., Al-Omari, Y. and Sahawneh, J., Ministry OF Energy and Mineral Resources.

Makhlouf, I.M. and Abed, A.M., 1991. Depositional facies and environments in the Umm Ishrin Sandstone Formation, Dead Sea area, Jordan. Sedimentary Geology, 71(3-4), pp.177-187.

Migoń, P., Goudie, A., Allison, R. and Rosser, N., 2005. The origin and evolution of foot slope ramps in the sandstone desert environment of south-west Jordan. Journal of arid environments, 60(2), pp.303-320.

Montes-Herrera, J.C., Cimoli, E., Cummings, V., Hill, N., Lucieer, A. and Lucieer, V., 2021. Underwater Hyperspectral Imaging (UHI): a review of systems and applications for proximal seafloor ecosystem studies. Remote Sensing, 13(17), p.3451.

Nayak, P.S. and Singh, B.K., 2007. Instrumental characterization of clay by XRF, XRD and FTIR. Bulletin of Materials Science, 30(3), pp.235-238.

Nimry, Y. and Haddadin, M., 1970. Glass sand of Ras El-Naqab. Report on Phase, 1.

NOAA,2018. [https://repository. library. noaa. gov/view/noaa/ 25214/ noaa_25214_DS1.pdf], [date of visit 25/6/2018].

Potts, P.J. and West, M. eds., 2008. Portable X-ray fluorescence spectrometry: Capabilities for in situ analysis. Royal Society of Chemistry.

Richards, J.A. and Richards, J.A., 1999. Remote sensing digital image analysis (Vol. 3, pp. 10-38). Berlin: Springer.

Royal Cultural Center., 1995. Remote Sensing Uses. Third Jordanian Scientific Week, Volume II: Scientific Papers (Theme of Mineral Wealth).

Saffarini, G., 1988. Ferried elements abundance in the carbonate-hosted iron occurrences of Jordan. Dirasat (Science), 15(9), pp.190-202.

Saibi, H., Bersi, M., Mia, M.B., Saadi, N.M., Al Bloushi, K.M.S. and Avakian, R.W., 2018. Applications of remote sensing in geoscience. In, Hung. M., Wu, Yi-Hwa (eds) Recent Advances and Applications in Remote Sensing, pp.181-203.

Salimi, A., Ziaii, M., Amiri, A., Zadeh, M.H., Karimpouli, S. and Moradkhani, M., 2018. Using a feature subset selection method and support vector machine to address curse of dimensionality and redundancy in Hyperion hyperspectral data classification. The Egyptian Journal of Remote Sensing and Space Science, 21(1), pp.27-36.

Scanvic, J. Y., 1997. Aerospatiale remote sensing in geology. CRC Press, 280P.

Sentinel Hub.2021. [www.Sentinel-hub.com. [Date of visit 10/8/2020].

Shakrour, O., Tarawneh, K. and Jamal, D., 2010. Exploration, evaluation and investment opportunities of feldspar ore deposits in Jordan. In 6th Jordanian International Mining Conference.

Sharp, R.P., 1988. Earth science field work: Role and status. Annual Review of Earth and Planetary Sciences, 16(1), pp.1-20.

Sivakumar, M., Roy, P., Harmsen, K. Saha, S., 2004. Satellite remote sensing and GIS applications in agricultural meteorology. Proceedings of the Training Workshop 7-11 July, 2003, Dehra Dun, India.

Treitz, P. and Rogan, J., 2004. Remote sensing for mapping and monitoring land-cover and land-use change-an introduction. Progress in planning, 61(4), pp.269-279.

Skauli, T., 2011. Sensor noise informed representation of hyperspectral data with benefits for image storage and processing," Opt. Exp., vol. 19, no. 14, pp. 13 031–13 046, Jul. 2011.

Trinity College Dublin. 2018. [www.tcd.ie/Geology/ undergraduate/ fieldwork.php], [date of visit 20/9/2020].

USGS, 2022. [https://www.usgs.gov/science/remote-sensing-minerals], [date of visit 19/1/2022].

USGS.2021.[https://www.usgs.gov/centers/eros/science/usgs-eros-archive-earth-observing-one-eo-1-hyperion], [date of visit 12/1/2021].

Viallefont-Robinet, F., Bacour, C., Bouvet, M., Kheireddine, M., Ouhssain, M., Idoughi, R., Grignon, L., Munesa, E., Lemaître, F. and Rivière, T., 2019. Contribution to sandy site characterization: Spectro-directional signature, grain size distribution and mineralogy extracted from sand samples.